4-1-2021

Influence of chitosan and hydroxyapatite incorporation on properties of electrospun PVA/HA nanofibrous mats for bone tissue regeneration: Nanofibers optimization and in-vitro assessment

samar A. salim
The British University in Egypt, samar.salim@bue.edu.eg

Samah A Loutfy

Esmail M El-Fakharany

Tarek H Taha

Yasmen Hussien

See next page for additional authors

Journal of Drug Delivery Science and Technology 62 (2021) 102417

Contents lists available at ScienceDirect

Journal of Drug Delivery Science and Technology

journal homepage: www.elsevier.com/locate/jddst

Research paper

Influence of chitosan and hydroxyapatite incorporation on properties of electrospun PVA/HA nanofibrous mats for bone tissue regeneration: Nanofibers optimization and *in-vitro assessment*

Samar A. Salim [a], Samah A. Loutfy [a,b], Esmail M. El-Fakharany [c], Tarek H. Taha [d], Yasmen Hussien [a], Elbadawy A. Kamoun [a,e,*]

[a] *Nanotechnology Research Center (NTRC), The British University in Egypt (BUE), El-Sherouk City, Cairo, 11837, Egypt*
[b] *Virology and Immunology Unit, Cancer Biology Department, National Cancer Institute, Cairo University, Egypt*
[c] *Protein Research Dep, Genetic Engineering and Biotechnology Research Institute (GEBRI), City of Scientific Research and Technological Applications (SRTA-City), Alexandria, 21934, Egypt*
[d] *Environmental Biotechnology Dep, Genetic Engineering and Biotechnology Research Institute (GEBRI), City of Scientific Research and Technological Applications (SRTA-City), Alexandria, 21934, Egypt*
[e] *Polymeric Materials Research Dep., Advanced Technology and New Materials Research Institute (ATNMRI), City of Scientific Research and Technological Applications (SRTA-City), New Borg Al-Arab City, 21934, Alexandria, Egypt*

ARTICLE INFO

Keywords:
PVA-Hyaluronic acid
Chitosan
Hydroxyapatite
Nanofibers
Tissue regeneration

ABSTRACT

3D-scaffolds composed of polyvinyl alcohol-hyaluronan (PVA/HA) nanofiber mats were fabricated by electrospinner. Spinning conditions of PVA/HA were optimized for obtaining uniform and smooth nanofibers (NFs). Resultant NFs were investigated by SEM, FT-IR and mechanical tensile. Chitosan was incorporated into NFs mats during spinning for reducing bleeding, microbial growth of wound bed, and enhancing viability/proliferation of cells in damaged tissues. Hydroxyapatite (HAP) after silanization using (3-aminopropyl)triethoxysilane (APTES) was also incorporated into scaffolds due to its similar chemical composition with mineral composition of bone, which stimulates interactions between bone tissue and biomaterial resulting in a prominent interface after implantation. NFs with different compositions were bio-evaluated *in vitro* using antimicrobial activity, hemolysis (%), cytotoxicity, and cell adhesion tests. Results revealed that, addition of HAP into PVA/HA mats improved significantly their mechanical/thermal stability and relatively hindered swelling index, compared to mats without HAP. However, addition of chitosan enhanced swelling index and antimicrobial activity of mats. All tested mats with different compositions showed high cell-viability, regardless incubation time or concentration of tested nanofibers. *In-vitro* cell adhesion results indicated that, WI38 cells adhered and proliferated adequately with nanofibers containing HAP. Such findings support the ability for using PVA/HA/CH/HAP NFs as biomaterials for bone tissue regeneration soon.

1. Introduction

Nowadays, bone tissue damages and injuries that can be happened in several body parts are popular health problems in our daily life [1]. For many years, allograft and auto-graft are major procedures being used to care damaged tissues in orthopedic surgeries [2]. However, these procedures have several disadvantages like; unavailability of donor, graft versus host reaction, and possibility of transmission of disease and unfavorable outcome. In addition of shortage of transplant sources and the defect can be occurred on the donor part of the body with probability of rejection of donated part and high chance of diseases transition [3]. Due to all of these limitations, researchers have been evoked to look for other strategies that help in repairing damaged tissues and organs in a safer way [4]. The first approach includes using expanded mesenchymal stem cells of stem cell concentrate to be on step procedure for the injection topically in the site of injury or defect [5]. However, such method showed unsuitability as it needs simple injuries, not complex structure like bone. The second approach involves using biodegradable scaffolds fabricated from different biomaterials, like natural polymers *e.g.* poly (lactic acid) (PLA) [6], collagen [7] and silk [8], synthetic polymers such

* Corresponding author. Nanotechnology Research Center (NTRC), The British University in Egypt (BUE), El-Sherouk City, Cairo, 11837, Egypt.
E-mail addresses: badawykamoun@yahoo.com, e-b.kamoun@tu-bs.de (E.A. Kamoun).

https://doi.org/10.1016/j.jddst.2021.102417
Received 3 October 2020; Received in revised form 3 February 2021; Accepted 5 February 2021
Available online 10 February 2021

as poly ethersulfone (PES)/polyaniline (PANI) [9]; as well as polycaprolactone (PCL) [10]. These polymers could be used to accelerate cell proliferation or used in conjugation with nanoparticles, growth factors and bioceramics [11]. Selection of polymer depends on both target application and degree of degradation. The last approach and the most effective method are using biodegradable and biocompatible scaffolds in combination with growth factors and specific material which is close to the chemical composition of mineral parts of bone [12]. The main goal of scaffolds is providing a better environment which is suitable for cell proliferation in addition to differentiation [13,14]. The proposed scaffolds aim to develop environmentally suitable scaffolds able to embed cells for treating bone defects, moreover; improving the mechanical properties which are an essential for process of bone regeneration. Thus, previous reported polymeric scaffolds showed remarked role for bone tissue engineering and cartilage repair [12–14].

Polyvinyl alcohol (PVA) is a synthetic polymer, water-soluble and easily spun for accepted morphological scaffold mats, without droplets formed during spinning process. In addition, PVA has adhesive quality, biocompatible and biodegradable properties. PVA mats were used with several polymers for impeding their application in medicine, and also raise the hydrophilicity of the arranged fibers [15]. Recently, chitosan is well-known to be the suitable nominee for the fabrication of appropriate biodegradable scaffolds.

Chitosan is a natural polysaccharide, it possesses several featured properties like: biocompatibility, bio-degradability, high performance characteristics and unique structure; therefore it has attracted researcher's attention to be used in many industries specifically in biomedical applications [16]. One of its relevant properties is, its cationic nature which allows its use as temporary scaffold to stimulate growth of regenerated tissues [17], its biological properties as anticancer, antimicrobial, anti-inflammatory, biotic adhesion, and its antioxidants activities [18]. Furthermore, the unique natural biopolymer which recently has gained more consideration is hyaluronic acid (HA) or hyaluronan. HA has attracted much attention for its natural presence in ECM (extracellular matrix) and its biocompatibility. Therefore, its clinical relevance allows its application in fabrication of wound dressings [19], skin substitutes [20], as well as joint lubricants [21]. HA is used for post-surgical adhesion as a pre-hydrophilic coating in post-surgical adhesion inhibition for cancer treatment [22].

Calcium phosphate nanoparticles or hydroxyapatite (HAP) $Ca_{10}(PO_4)_6(OH)_2$ has chemical composition is close to bone tissue composition. Therefore, it can be used as scaffold with a capability of tissue renewal and regeneration [23]. HAP is considered as one of the best compounds with *osteo-inductive* properties which present naturally in bone structure [24]. Previously, HAP was used to induce interactions between bone tissue and biomaterial forming adequate interface after implantation. However, HAP showed bone growth on their surface and partial bioactivity; therefore a promising way to improve their bioactivity is *via* functionalization of HAP with free amino groups which can be resulted from its binding with organic anchors ((3-Aminopropyl) triethoxysilane) (APTES) [25]. Previously, PVA/CH/HAP-loaded TWS119 drug scaffold was synthesized for accelerating bone regeneration, where this study demonstrated that HAP incorporation improved bioactivity of scaffolds and chitosan facilitated for producing a scaffold with antibacterial activity for bone tissue regeneration system [26].

Herein, for the first time in literature; PVA-HA–CH–HAP nanofibrous scaffolds were fabricated by electrospinning technique, while spinning conditions of scaffolds ingredients among each other, were comprehensively studied and explained in detail. The impact of blending of nanofibrous compositions *e.g.* chitosan and hydroxyapatite nanoparticles on the resultant nanofibers properties were studied in terms of physicochemical properties, biocompatibility of nanofibers as new biomaterials for bone tissue regeneration purposes.

2. Materials and methods

2.1. Materials

Polyvinyl alcohol (PVA, M_{wt} = 72,000 g/mol; 86% hydrolyzed) was purchased from Loba Chemie, India. Chitosan (CH) (deacetylation degree < 86%, $M_n \sim 4.5 \times 10^5$) was obtained from Ruji Biotech Development Co., Ltd., Shanghai, China. Hyaluronic acid (HA) (M_{wt} = 10,000–15,000 g/mol) was purchased from Shanghai Jiaoyuan Industry Co., Ltd, Shanghai, China. Nano-Hydroxyapatite (HAP) (<200 nm particle size (BET) containing 5 wt, % silica as dopant) and 3-aminopropyltriethoxysilane (APTES) were obtained from Sigma Aldrich, Missouri, USA. Citric acid anhydrous (CA) was obtained from Sigma-Aldrich Chemie GmbH, Steinheim, Germany. Glacial acetic acid was obtained from Fisher Scientific, USA. Electrospinner unite model: (MECC, NANON-01A, Japan) was used for fabricating electrospun nanofibrous mats.

2.2. Functionalization of hydroxyapatite (HAP)

Hydroxyapatite nanoparticles were functionalized based on procedure of Russo et al. [25], as reported elsewhere. Typically, 5.6 g of HAP was well-dispersed in 50 ml of distilled water under stirring for 2 h at 60 °C, to allow hydrolysis of alkoxy groups of HAP. Afterwards, 2 ml of modifier agent (APTES) was added dropwise (one ml/15 min) to get HAP suspension solution. The HAP suspension solution was reserved under stirring overnight at 60 °C. HAP-APTES suspension solution was centrifuged at 3000 rpm for 30 min, followed by washing the modified HAP residues with hot-distilled water for several times. The purification or washing step was repeated at least three times to eliminate an overload or unreacted APTES. The resultant modified HAP was dried in oven at 60 °C for 6 h, and then compressed the resultant organic HAP by mortar and dry stored for further uses.

2.3. Fabrication of PVA/HA/CH/HAP nanofiber scaffolds

Briefly, (10%, w/v) of PVA was dissolved in 10 ml of distilled water with harsh stirring for overnight at 60 °C. A 2% (w/v) of HA was separately dissolved at room temperature for 12 h, meanwhile (1.5% (w/v) of chitosan was dissolved in 0.5% (v/v) glacial acetic acid-water at ambient temperature for 5 h with continuous stirring. The blend ratio of (PVA/HA) solution as (8.2 : 1.8 ml) (v/v) was mixed together and kept under stirring at 50 °C for further 3 h till getting homogenous one-phase mixture. A 0.15 g (1.5%, w/v) of citric acid as crosslinker was

Table 1
Optimization of spinning conditions for fabricating PVA/HA, PVA/HA/CH, PVA/HA/HAP, and PVA/HA/CH/HAP nanofibrous scaffolds.

PVA:HA ratio	PVA concentration (%, w/v)	HA concentration (%, w/v)	Voltage (kv)	Feed rate (mL/hr)	Distance between tip &collector (cm)	Nanofiber morphology observation
8 : 2	10	4	28	0.5	15	No nanofibers formed
8 : 2	10	2	28	0.2	15	Fibers formed with some beads
6 : 4	10	2	28	0.2	15	Ribbon-shape nanofibers formed
5 : 5	10	2	28	0.1	15	Poor nanofibers formed
8.2 : 1.8	**10**	**2**	**28**	**0.3**	**15**	**Beads-free nanofibers**

Bold cells mean the chosen optimized conditions for obtaining uniform nanofibers.

added at related to the total amount of polymers (*i.e.* 10 ml); PVA/HA-citric acid mixture solution was kept under stirring at room temperature for 30 min. Chitosan was incorporated into PVA/HA to form PVA/HA/CH scaffold in ratios (8.2: 1.8: 2.5 ml) (v/v), respectively; where the latter solution was crosslinked using citric acid at room temperature then remained under stirred for 2 h, followed by ultrasonicated for 15 min before spinning. The bioactive silanized-HAP nanoparticles were incorporated in ratio of (1.0 wt%) into PVA/HA, or PVA/HA/CH (PVA/HA/CH/HAP viscosity 6.25 ± 0.75 Pa s, conductivity 410 ± 5.25 μS cm^{-1}, and surface tension 125 ± 1.5 Mn. m^{-1}). Accordingly, different scaffolds composed of (PVA/HA, PVA/HA/CH, PVA/HA/HAP, and PVA/HA/CH/HAP) crosslinked by citric acid nanofibrous mats were fabricated by electrospinner (model: MECC, NANON-01A, Japan). The polymer solution was withdrawn into 5 ml syringe (equipped with 22G needle). Electrospinning was performed in varying operating regimes as feeding rate ranged between (0.1–0.5 ml/h), and operating voltages ranged 28–30 Kv. All NFs samples were electrospun at ambient conditions with humidity of ~55% (Table 1). Produced nanofibers were thermally treated at 60 °C for further 6 h and one hour at 85 °C.

2.4. Instrumental characterizations of nanofiber scaffolds

SEM: The morphology of nanofiber surfaces with different mats compositions was investigated by scanning electron microscope (**SEM**, Joel GSM-6610LV, Japan). All samples were investigated without coating with gold-thin layer under low vacuum and low voltage at 5 Kv to avoid samples-shrinkage and deformation. **FTIR**: The chemical composition of PVA/HA, PVA/HA/CH, PVA/HA/HAP and PVA/HA/CH/HAP scaffolds was analyzed by FTIR (IR, 8400s Shimadzu, Japan) with IR Finger-prints recorded 4000-400 cm^{-1}. **TGA**: Thermal degradation of different mats was tested by thermogravimetric analysis (TGA-50, Shimadzu, Japan). Dried nanofibers were operated under nitrogen gas at heating rate of 10 °C/min at a temperature ranged 0–500 °C.

Mechanical strength: Tensile strength of different composition of scaffolds was measured by standard uniaxial tensile test (Z050, Zwick Roell AG, Ulm, Germany). The mechanical parameters of scaffolds *e.g.* maximum strength, elongation-to-break (%) and Young's modulus were measured for all tested scaffolds.

2.5. Physicochemical properties of nanofiber scaffolds

2.5.1. Swelling index (SI)

Scaffolds were weighed separately (W_1) and soaked in a *Petri-dish* (100 mm × 15 mm) containing 10 ml deionized water. After 5 min, samples were removed and the extra water was wiped by soft towels paper. Swollen mats were re-weighed (W_2) at time-intervals against the change of sample mass, as displayed in equation (1).

$$SI = ((W2 - W1))/W1 \quad (1)$$

2.5.2. Protein adsorption of nanofiber scaffolds

The amount of adsorbed bovine serum albumin (BSA) onto scaffolds surfaces was measured by UV–Vis spectrophotometer at 630 nm, using standard calibration curve of BSA ranged concentrations (3–60 mg/ml). The exact adsorbed BSA onto scaffold surface was calculated by Beer's law according to equation (2).

$$A = acL \quad (2)$$

Where, (A) is the absorbance, (a) is a proportionality constant, (c) is the concentration, and (L) is the path length which is constant [27]. Sections of different scaffolds were cut into (1 cm × 1 cm) after that these pieces were immersed into 10 ml of PBS (pH ~ 7.4), and incubated at 37 °C for 24 h until equilibrium swelling weight was obtained. The swollen hydrogel pieces were transferred to buffer solution containing BSA (30 mg/ml) and shacked for 4 h at 37 °C, and then the scaffolds sections were slightly removed. The adsorbed protein was calculated by difference between protein concentrations before and after soaking nanofiber parts in protein/PBS using albumin reagent kit (at 630 nm). This procedure has been slightly adjusted from the previous described method of Lin et al. [28].

2.5.3. Antimicrobial activity of nanofiber scaffolds

The antimicrobial activity of composite nanofibers was investigated against eight human pathogenic microbes using disc diffusion method [29]. Scaffolds were first sanitized using UV lamp for 30 min, directly before start the microbial test. Typically, Luria Bertani (LB) agar was freshly prepared, sanitized, poured in Petri plates, and then solidified under aseptic conditions. On the other hand, eight pathogenic microbes (*Vibrio cholerae* ATCC700, *Candida albicans* ATCC 700, *Pseudomonas aeruginosa* ATCC9027, *Escherichia coli* NCTC10418, *Klebsiella pneumoniae* ATCC13883, *Bacillus cereus* ATCC6633, *Staphylococcus aureus* ATCC6538, and *Streptococcus mutans* ATCC25175) were separately cultivated into 5 ml of LB broth and incubated at 30 °C under gentle agitation at150 rpm for 18 h. Each microbial culture was diluted to 0.5 McFarland standard and spread over LB agar plates by sterile-cotton swabs. The composite nanofibers discs were prepared in 0.7 mm diameter and loaded over the inoculated plates. All plates were incubated at 30 °C for 24 h, and the inhibition clear zones were measured and recorded [29].

2.5.4. Haemocompatibility of nanofiber scaffolds

The hemolysis test is almost performed to investigate the biocompatibility of specific material. It depends on the ability/inability of a tested material to lye the RBCs of a healthy person and releasing its hemoglobin content [29]. The test is performed by addition of 10 μl of whole human blood to 700 μl of Ca^{+2}-Mg^{+2} free DPBS buffer. After well mixing, one disc of each tested nanofiber was separately added followed by incubation of the whole mixture at 37 °C for 3.5 h with interval inverting every 30 min. The positive and negative controls were respectively prepared using 100 μl Triton X-100 and 100 μl DMSO (0.5%) instead of tested nanofiber discs. After incubation, all tested tubes and controls were centrifuged at 10.000 rpm for 15 min. A ten-fold diluted cyanmethemoglobin reagent was mixed in a percentage of 1:1 with the contents of each tested tube and controls, separately. The absorbance of all tested samples and controls were measured at 540 nm using UV–Vis spectrophotometer against blank (Ca^{+2}-Mg^{+2} free DPBS buffer plus sample without blood).

2.5.5. Cytotoxicity of nanofiber scaffolds

All NFs with different composition *e.g.* (PVA/HA, PVA/HA/CH, PVA/HA/HAP, and PVA/HA/CH/HAP) were evaluated for their toxicity on WI38 (fibroblast cells derived from human lung tissue) using MTT assay, as previously demonstrated by Hussien et al. [29] In brief, WI38 cells (1.0×10^3) were seeded in sterile 96-well flat bottom micro-plates and cultured in DMEM media (Lonza, USA) supplemented with 10% fetal bovine serum (FBS) for 24 h at 37 °C in 5% CO_2 incubator. Then, different discs from all tested NFs at weights of 1.0, 2.0, 3.0, 4.0 and 5.0 mg/ml, were added to cells and incubated at 37 °C in 5% CO_2 incubator for 1, 3, and 5 days. After washing cells three times with fresh media to remove debris and dead cells, 200 μl of MTT solution was added to each well at concentration of 0.5 mg/ml and incubated for 2–3 h at 37 °C in 5% CO_2-incubator. After discarding MTT solution, the formed formazan crystals were dissolved in 200 μL/well of DMSO. All plates were measured at 630 nm and subtracted from measuring at 570 nm using a micro-plate ELISA reader. All tests were performed in triplicates and the relative cell viability (%), compared to control wells containing cells without treatment was calculated using the following formula: (A) test/(B) control × 100% [29].

2.5.6. Cell adhesion test onto nanofiber scaffolds

Nanofiber scaffolds underwent to coat the surface of wells by adding discs at different concentrations in 1.0 ml/well of PBS to 24-well plates

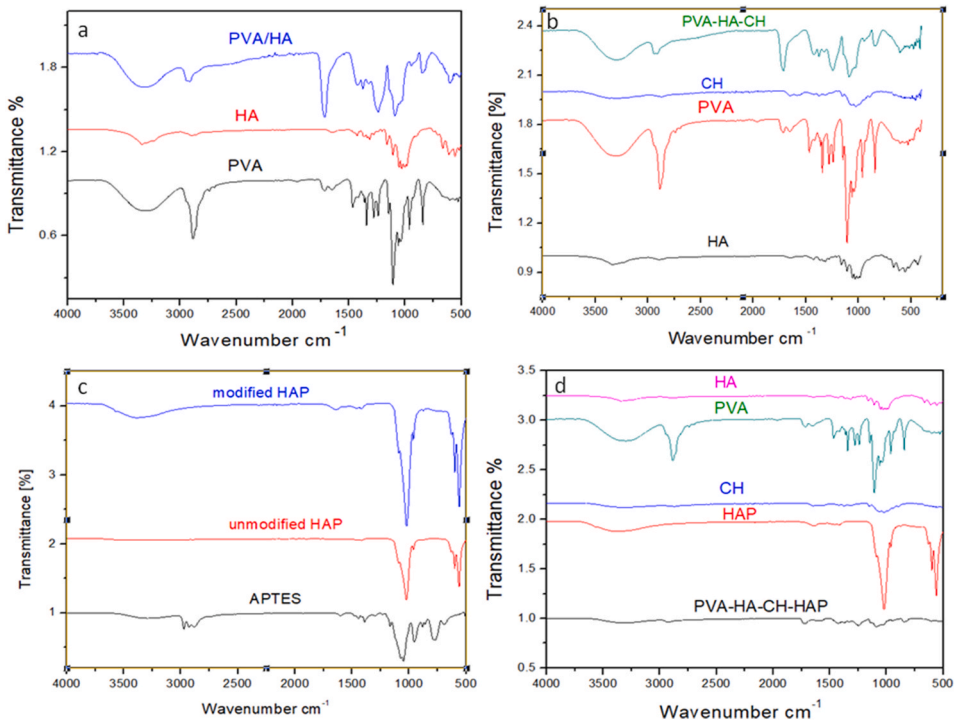

Fig. 1. FT-IR spectra of NFs scaffolds of **(a):** (PVA, HA and PVA/HA), **(b):** (PVA/HA/CH), **(c):** (PVA/HA/HAP), and **(d):** (PVA/HA/CH/HAP and modification of hydroxyapatite with APTES).

in triplicates. After incubation for 72 h at ambient temperature, discs were taken out and wells were blocked by adding 1.0 ml of 10% BSA to each well, and then incubated for one hour at 37 °C. After washing, WI38 cells (1.0×10^6) were seeded into the blocked 24-well tissue culture plates in RPMI-1640 media supplemented with 10% FBS at 37 °C for (0.5, 2, 4 and 6 h). The number of attached cells was accounted by adding 0.5 ml/well of 0.1% (w/v) crystal violet solution and incubated at room temperature for 60 min. Then, cells were washed for three times with 1.0 M of PBS and the absorbance was measured at 570 nm by micro-plate ELISA reader [8,9,29].

3. Results and discussion

3.1. Optimization of spinning conditions

Recent findings reported different spinning conditions to obtain uniform and beads-less nanofibers [29]. For this purpose, different ratios of nanofiber composition blends were used; where *e.g.* PVA and HA were fabricated with different solution feeding rate, as shown in Table 1. Table 1 represents the optimization of spinning conditions for fabrication of different composite NFs scaffolds. Meanwhile, high voltage about 30 Kv and the distance between spinneret syringe-needle and aluminum foil-collected is about 15 cm, were kept constant as optimized condition values for getting accepted morphological nanofibers. It was noticed that, the feeding rate of polymer solution from syringe-needle showed to be one of the most important parameter that can control the topography of the formed nanofibers. It was found that, all uniform nanofibrous scaffolds were fabricated through the feeding rate at 0.3 ml/h, except the feed rate of PVA/HA/CH/HAP scaffold was adjusted at 0.2 ml/h. However, the feeding rates less or more 0.3 ml/h might result in formation of beads and polymer solution drops formed during spinning process or irregular nanofiber formation onto aluminum collector. The feeding rate at 0.3 ml/h was chosen as one of optimized conditions for the spinning process of PVA/HA NFs. The collected nanofibers mats were dried using dry oven at 60 °C for 2 h to eliminate residual solvents; also all scaffolds were kept in dried and cold conditions to avoid surrounded contamination or hydration. Interestingly, the blend ratio of PVA and HA solutions at (8.2: 1.8 ml, (v/v)) was chosen as the optimum ratio, due to obtaining uniform nanofibers with less beads formed during spinning process and accepted surface morphology of nanofibers, compared to other PVA:HA ratios. While, CH or HAP in case PVA/HA/CH and PVA/HA/HAP, respectively; was incorporated into polymer solution for spinning in one volume ratio without variation. All scaffolds were crosslinked using 0.15 g of citric acid (Table 1).

3.2. FTIR spectra of nanofibrous scaffolds

Fig. 1 shows FTIR spectra of fabricated (PVA/HA, PVA/HA/CH, PVA/HA/HAP and PVA/HA/CH/HAP) scaffolds. As seen, all spectra of scaffolds showed distinguished bands of PVA of hydroxyl group (-OH) at v 3200 cm^{-1}, alkyl group (-CH_2) at *v* 2850 cm^{-1}, as well as remained acetyl group (-C═O) at *v* 1700 cm^{-1}. After adding HA into PVA/HA scaffold, it resulted in a clearly appearance of –NH band at near *v* 1630 cm^{-1}, as shown in Fig. 1a, also the density of –OH group reduced in PVA/HA scaffold, comparing with PVA spectrum alone due to successful crosslinking between –OH in PVA and –COOH in citric acid crosslinker (Fig. 1a) [29]. Also, two vibration bands at near *v* ~1400 and 1340 cm^{-1} are corresponded to –NH_2 and –C–C, respectively; which were created by interaction between PVA and chitosan (Fig. 1b). On the same context, FTIR spectra of modification of HAP was described in Fig. 1c, where the salinization of HAP nanoparticles using APTES were verified by appearance of characteristic bands at near *v* 3400 cm^{-1}, which is corresponding to formation of Si–O, in addition to intensive absorption bands in region at *v* 1100 -1200 cm^{-1}, which are corresponding to asymmetric stretching of siloxane group Si–O–Si. Also, appearance of band at near *v* ~1390 cm^{-1} is corresponding to –NH_2 creation which is further verification for functionalization or silanization of HAP by APTES. In spectra of scaffold PVA/HA/HAP as shown in Fig. 1d, it was observed that presence of absorption band at near *v* ~2900 cm^{-1} is corresponding to –O-H and distinct bands at *v* ~559, and 1200 -550

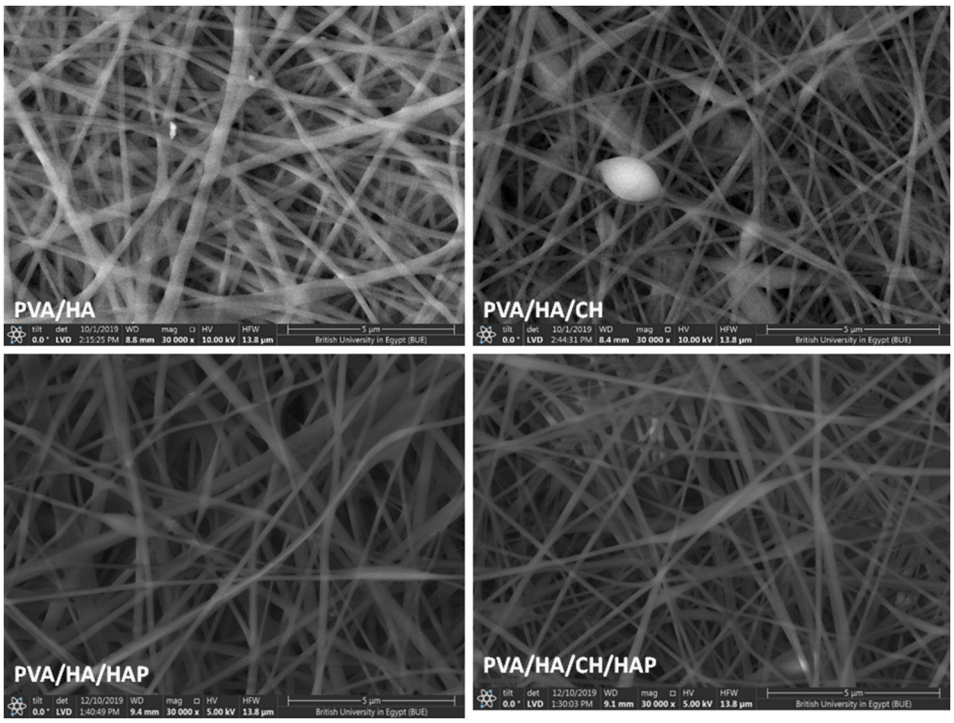

Fig. 2. SEM images of fabricated NFs scaffolds of (PVA/HA), (PVA/HA/CH), (PVA/HA/HAP), and (PVA/HA/CH/HAP) (*original magnification 30,000x at 10Kv with scale* 5 μm).

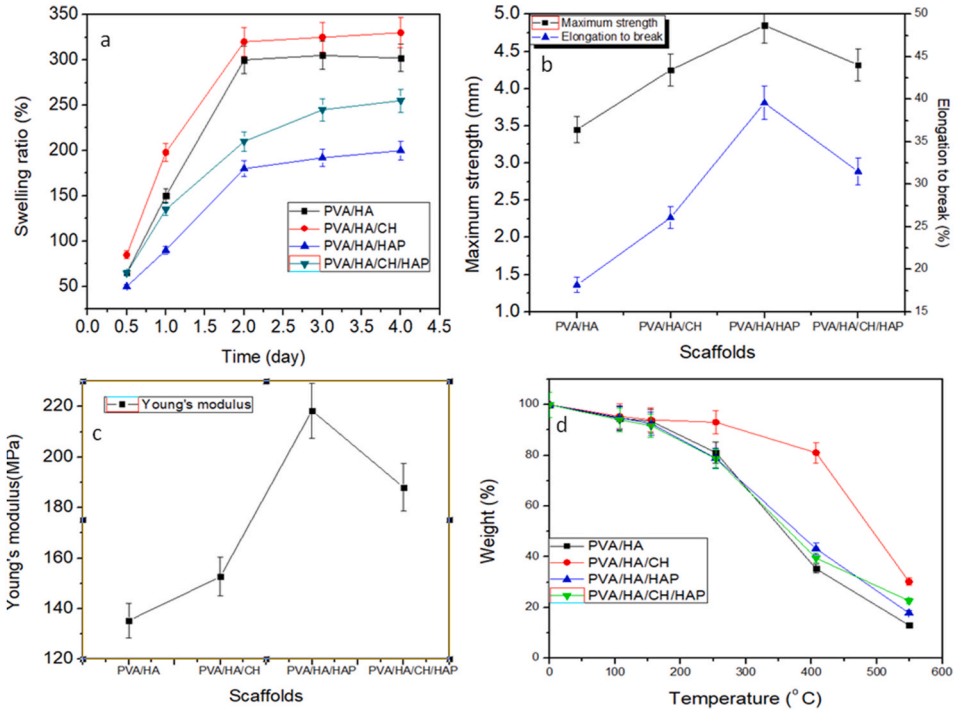

Fig. 3. Physicochemical properties of nanofibrous (PVA/HA), (PVA/HA/CH), (PVA/HA/HAP), and (PVA/HA/CH/HAP) scaffolds: Swelling ratio **(a)**, mechanical properties **(b** and **c)** (mean ± SD, n = 3, $P < 0.05$), and TGA thermographs **(d)**.

cm^{-1} for PO_4^{-3}. PVA/HA/CH/HAP spectrum shows a significant band at 1650 cm^{-1} of –NH which is specific for HA, distinct peaks near to *v* ~550 cm^{-1}, and 559 cm^{-1} are related to -PO_4^{-3} definite for HAP as well as presence of specific absorption bands of chitosan at *v* ~1400 cm^{-1} of $–NH_2$ groups. This indicates that the spectrum of PVA/HA/CH/HAP realized all characteristic spectrum peaks of all mats compositions.

3.3. Morphology investigation of nanofibrous scaffolds

SEM investigation always is employed for providing topographical data and surface structural characteristics of nanofibers. Fig. 2 illustrates surface morphology investigation of different composition of nanofibrous scaffolds. It was clearly observed that morphological features

alteration according to the compositions of each scaffold. As can be revealed in Fig. 2, addition of HAP to PVA/HA induced the morphology of scaffold, where HAP bounded by PVA creates less porous area, tiny pores distribution, few beads and clear/uniform fibrous structure formed. Such morphology of 3D-scaffold is quiet relevant for vascularization, as scaffolds surface possesses filamentous and interconnected pores, particularly scaffolds containing HAP. Previously, incorporation of HAP particles improved adhesion ability of body cells and encouraged differentiation; in addition, it enhanced proliferation of cells into the body especially osteoblasts and *mesenchymal* cells to submit *osteogenesis* [30]. In addition, chitosan allowed for creation of more pores, and perhaps wide pores and crakes formation onto scaffold surface as observed in Fig. 2b and d. Thus, nanofibrous scaffolds containing HAP nanoparticles provided high mechanical stability and compacted surface strictures, as proven in Fig. 2. Whereas, nanofibrous scaffolds containing chitosan displayed high swelling ability due to presence of high pores contents as proven in Fig. 3a. Our results are agreed with results of Agrawal et al. [31] they proved that addition of chitosan dramatically affected the morphological structure of PVA/CH nanofibers through increasing porosity of mats surface and decreasing nanofibers diameter.

3.4. Swelling study

Swelling study of resultant nanofibers is considered one of fundamental parameters for biomaterials, as well as the swellability degree as scaffold is designed to be used under high humidity condition. To achieve this theory for adequate cell nutrition and cell signaling, scaffolds were soaked up water through their porous network at 37 °C [32]. Significant differences were detected in the tested four scaffolds groups (PVA/HA, PVA/HA/CH, PVA/HA/HAP, PVA/HA/CH/HAP) as shown in Fig. 3a. It was noticed that, PVA/HA/CH reached to a high degree of swelling ratio ~325%, comparing to PVA/HA at ~300% after 2 days of equilibrium swelling rate. This might be attributed to presence of chitosan (*i.e.* PVA/HA/CH) which possesses hydrophilic group's *e.g.* amino groups that allowed penetration of water molecules inside scaffolds chains. Therefore, this scaffold showed the highest hydrophilicity and swellability, compared to other tested scaffolds. After incorporating salinized-HAP nanoparticles into nanofibers, it was observed that HAP incorporation decreased significantly the swelling ability of nanofibers, compared to PVA/HA/CH scaffold. As seen, PVA/HA/HAP nanofibers showed swelling ratio (%) of ~170% after 2 days of swelling; however, the addition of chitosan into the latter nanofibers (PVA/HA/CH/HAP nanofibers) reached to swelling ratio ~ 240%, after prolonged swelling time to 4 days. This implies that HAP incorporation into nanofibers reduced significantly the swelling rate, due to the interaction between HAP nanoparticles with –OH groups of PVA and HA which resulted in swelling reduction. On the contrary, chitosan incorporation into nanofibers might improve the swellability and penetration degree of nanofibers, due to high hydrophilicity of chitosan. The current results are consistent with previous results of Sergio and his coworkers [33], who demonstrated that using chitosan at high concentration increased significantly the degree of swelling of PVA/CH/HAP scaffolds cross-linked physically using freeze-thawing cycle's method.

3.5. Mechanical stability of nanofiber scaffolds

Young's modulus, elongation-at-break (%) and maximum strength of four tested scaffolds groups were measured to evaluate the behavior of scaffolds under mechanical loads, where results are presented in Fig. 3b and c. Interestingly, incorporation of HAP into PVA/HA and PVA/HA/CH nanofibers greatly enhanced the mechanical strength, compared to nanofibers without HAP *e.g.* PVA/HA and PVA/HA/CH nanofibers (Fig. 3b and c). It was noticed that, the incorporation of HAP enhanced the mechanical properties of NF scaffolds to the highest values in case PVA/HA/HAP (maximum strength 4.85 mm, and 40% elongation-at-break) and PVA/HA/CH/HAP (maximum strength 4.25 mm, and 32% elongation-at-break), compared to PVA/HA and PVA/HA/CH NF scaffolds. This indicates that, addition of chitosan might reduce mechanical stability of nanofibers to certain extent. Similarly, Young's modulus values of nanofibers enhanced clearly due to HAP nanoparticles incorporation; where Young's modulus of PVA/HA/HAP nanofibers reached to 218.4 ± 4.5 M pa., while it was sharply reduced to 188 ± 5.25 M pa due to chitosan was incorporated to nanofibers. However, Young's modulus values of nanofibers containing HAP nanoparticles (*i.e.* PVA/HA/HAP and PVA/HA/CH/HAP) were the highest compared to nanofibers without HAP (*i.e.* PVA/HA and PVA/HA/CH nanofibers) (Fig. 3c). These results highlight that the compatibility between PVA, HA and CH with HAP has been realized as result of blending mechanism. Meanwhile, addition of HAP to the polymer solution created a well-porous interconnected material which improves mechanical properties of scaffolds, and in turn facilitates cell adhesion, proliferation and differentiation. These results are consistent with Ghiska et al. [34], where mechanical properties *e.g.* (Young's modulus value) of PVA/CH/HAP scaffold physically-crosslinked by freeze-thawing method, increased clearly from 143 to 191 M pa., due to incorporation of HAP nanoparticles into PVA/CH matrices from 25 to 40 wt %, respectively [34].

Table 2
Thermal stability data of nanofibrous scaffolds adapted from TGA thermograph results.

Nanofibrous scaffold composition	T_{onset} °C	T_{50}. (°C) of 50% weight loss	1st Decomposition stage °C, (weight loss, %)	2nd Decomposition stage °C, (Weight loss, %)
PVA/HA	254	407	100–254 13%	254–549 67%
PVA/HA/CH	277	416	100–277 13%	277–549 62%
PVA/HA/HAP	288	522	100–288 15%	288–549 63%
PVA/HA/CH/HAP	306	491	100–306 15%	306–549 60%

3.6. Thermal stability by TGA of nanofibrous scaffolds

TGA measurements were conducted for tested four nanofibrous scaffold groups, where TGA thermographs were drawn in Fig. 3d, while the thermal data were summarized in Table 2. Results showed that at temperature less than 100 °C; a slight loss of weight in all samples was detected which is related to removal of moisture, humidity, or solvent traces in different mats. TGA graphs confirmed that both scaffolds that contained hydroxyapatite (*i.e.* PVA/HA/HAP and PVA/HA/CH/HAP) showed remarked increase in T_{onset} values (288 and 306 °C), respectively, compared to control mats (PVA/HA and PVA/HA/CH) at (254 and 277 °C), respectively. As well the scaffolds (PVA/HA/HAP and PVA/HA/CH/HAP) revealed that the temperature at which 50% of their weight loss represented also a significant raise as (522 and 491 °C), respectively; compared to control scaffolds with HAP free (PVA/HA and PVA/HA/CH at 407 and 416 °C), respectively. These indicate that HAP incorporation into scaffolds proceeded as filler action, which in turns improved thermal stability of scaffolds compared to mats without HAP (Table 1). Likely, nanofibrous scaffolds containing HAP nanoparticles (PVA/HA and PVA/HA/CH) displayed adequate thermal stability during the second decomposition stage at (288 and 306 °C), respectively; compared to scaffolds without HAP (PVA/HA and PVA/HA/CH at 254 and 277 °C), respectively.

3.7. In vitro protein adsorption test

Adsorption of protein on the surface of foreign material is exposed directly to blood which showed to be relevant for adhesion and activation of platelets as reported by Burkovskaya et al. [35] Several

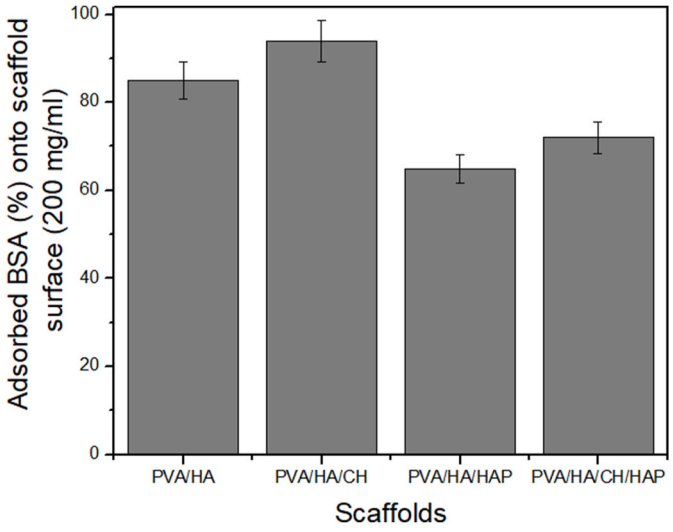

Fig. 4. Plots of adsorbed BSA onto the surface of NFs scaffolds of (PVA/HA), (PVA/HA/CH), (PVA/HA/HAP), and (PVA/HA/CH/HAP) at 37 °C.

Table 3
Antimicrobial activity of composite nanofiber scaffolds against human pathogenic bacteria and yeast.

Type of pathogenic microbes	Inhibition zone (mm)			
	PVA/HA	PVA/HA/CH	PVA/HA/HAP	PVA/HA/CH/HAP
Vibrio cholerae	0	0	0	0
Candida albicans	**10**	**11**	**10**	**10**
Pseudomonas aeruginosa	0	0	0	0
Escherichia coli	0	0	0	0
Klebsiella pneumoniae	**14**	**12**	0	0
Bacillus cereus	**14**	**11**	**10**	**8**
Staphylococcus aureus	0	0	0	0
Streptococcus mutans	0	0	0	0

physiochemical properties possess a vital role for controlling protein adsorption onto surface of nanofibers; for example, hydrophobicity of electrospun nanofiber, surface energy and electrostatic interaction between proteins and surface of nanofibers [36]. As shown in Fig. 4, PVA/HA/CH scaffolds exhibited the highest amount of BSA adsorbed (~94%) onto mats surface, compared to mats containing HAP nanoparticles with adsorbed BSA ranged ~ 65–72%. Interestingly, after addition of CH into PVA/HA/CH/HAP mats, CH improved BSA adsorption which increased to ~85%. This might be attributed to ability of CH to increase porosity of scaffold surface. Furthermore, its high degree of swelling as explained aforementioned in Fig. 3a and high porous surface mats was observed (Fig. 2). Where, BSA occupied all free available pores on the electrospun nanofibers based on probably hydrophilic surface interaction between chitosan and BSA. However, in case of scaffolds containing silanized-HAP nanoparticles might restrict adsorption of BSA onto mats surface. These results are agreed with results of Hwang et al. [37], who reported that protein adsorption increased with increasing blended hydrophilic biomaterial like alginate or dextran in PVA/dextran scaffold allowing its application as wound dressing materials.

3.8. Antimicrobial activity of nanofiber scaffolds

Antimicrobial activity of tested nanofibers was investigated against six human pathogenic bacteria and yeast. As shown in Table 3, the potency of the tested nanofibers to cease the microbial growth was varied significantly. Some of pathogens seem highly tolerant and was not

Table 4
Hemolysis percentage of composite nanofibers scaffolds against healthy human blood sample.

Type of nanofiber	Hemolysis (%)
PVA/HA	7.5
PVA/HA/CH	13.8
PVA/HA/HAP	83
PVA/HA/CH/HAP	28.3
Positive control	100

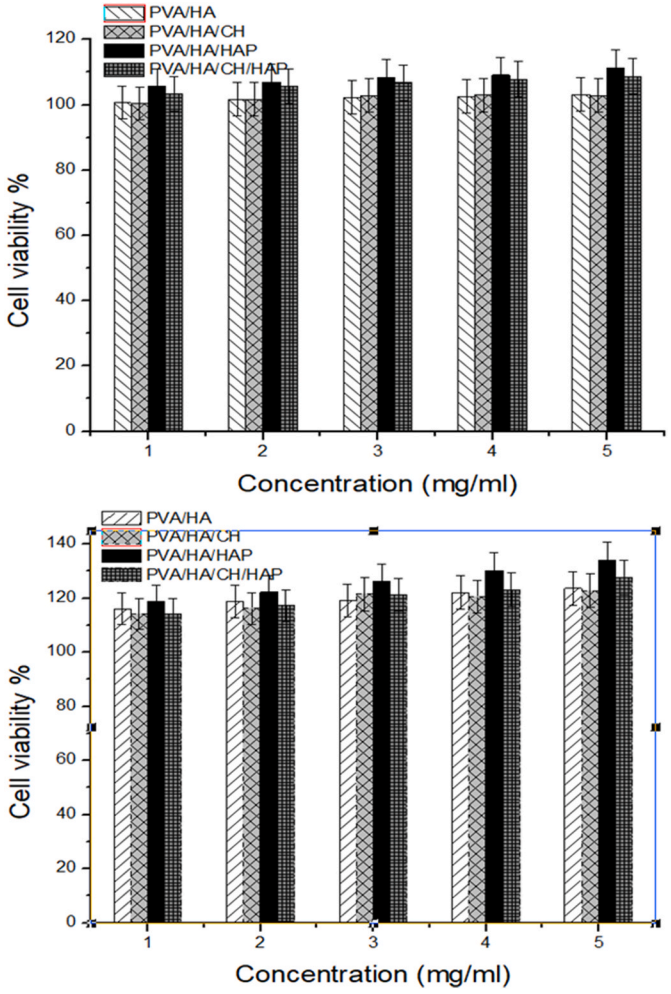

Fig. 5. Cell viability (%) of tested electrospun NFs of (PVA/HA), (PVA/HA/CH), (PVA/HA/HAP), and (PVA/HA/CH/HAP) scaffolds on *WI38* cell line after one day of incubation *(up)* and after 5 days of incubation *(down)*, (mean ± SD, n = 3, $P < 0.05$).

affected by the four tested nanofibers *e.g. Vibrio cholera, Pseudomonas aeruginosa, Escherichia coli, Staphylococcus aureus* and *Streptococcus mutans*. However, others scaffolds were inhibited the microbial growth like, *Candida albicans* and *Bacillus cereus*. A moderate effect of growth inhibition was observed for *Klebsiella pneumonia.* Among the tested material, PVA/HA was observed to be the most potent antimicrobial agent that showed clear zones from 10 to 14 mm against *Candida albicans*, *Klebsiella pneumonia* and *Bacillus cereus*. On the other hand, other tested materials exhibited similar antimicrobial activity with clear zones ranged from ~11, 12, 10, and 8–10 mm for PVA/HA,PVA/HA/HAP, and PVA/HA/CH/HAP, respectively. It could be concluded that the antimicrobial activity of the four tested nanofibers follows the following pattern order: PVA/HA ˃ PVA/HA/CH ˃ PVA/HA/HAP ≥ PVA/HA/CH/HAP. This implies that composite nanofibers scaffolds containing HAP

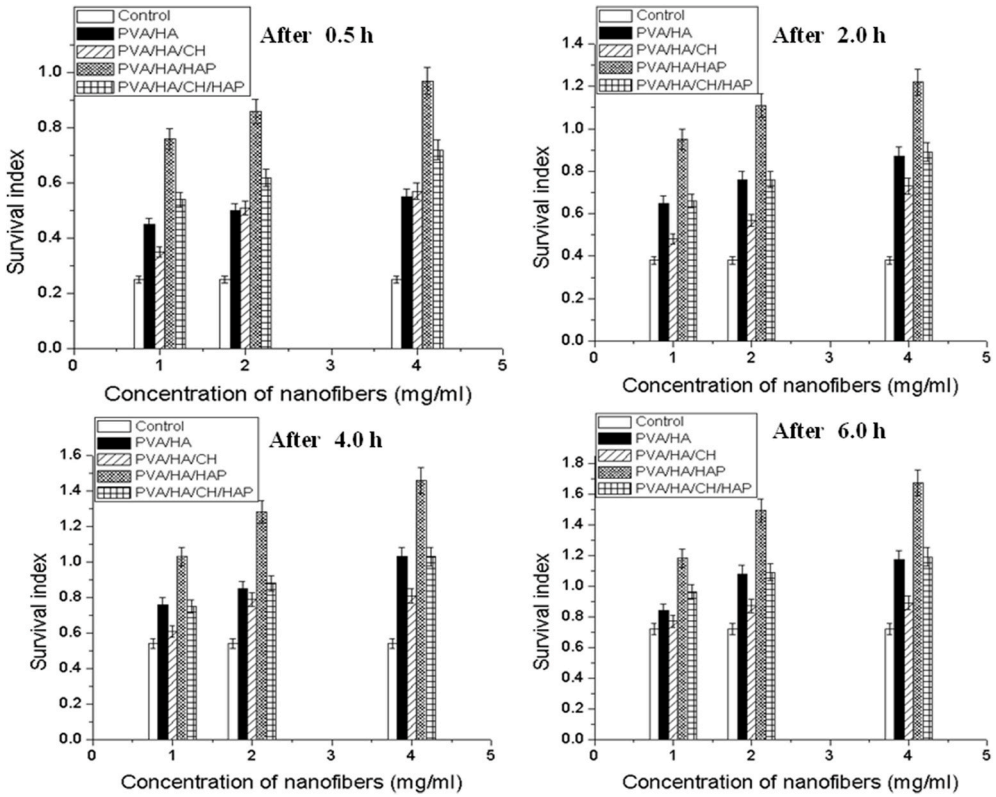

Fig. 6. Cell adhesion test of (PVA/HA), (PVA/HA/CH), (PVA/HA/HAP), and (PVA/HA/CH/HAP) NFs scaffolds using three NFs concentrations 1, 2, 3, 4, and 5.0 (mg/ml) after (0.5, 2, 4, and 6 h) of incubation (mean ± SD, n = 3, $P < 0.05$).

nanoparticles showed a relative microbial resistivity, owing to presence of HAP nanoparticles which might hinder the diffusion of test media and in turn affected antimicrobial activity of the tested nanocomposite.

3.9. Haemocompatibility of nanofiber scaffolds

The prepared nanofibers scaffolds were screened for their ability to disrupt the RBCs of a healthy blood and releasing their hemoglobin content [29]. Obtained results revealed that, all tested nanofibers are varied in their hemolysis behavior in a pattern lower than the hemolysis value recorded by the positive control. As shown in Table 4, the hemolysis percentages of PVA/HA, PVA/HA/CH, and PVA/HA/CH/HAP nanofibers were lower (7.5, 13.8 and 28.3%, respectively) than the hemolysis percentage of PVA/HA/HAP (~83%) nanofiber. Therefore, the safety of tested nanofibers towards RBCs obtained from blood of a healthy individual could be presented as follows PVA/HA ˃ PVA/HA/CH ˃ PVA/HA/CH/HAP ˃ PVA/HA/HAP.

3.10. Cytotoxicity of nanofiber scaffolds

Results demonstrate that all tested NFs ((PVA/HA, PVA/HA/CH, PVA/HA/HAP, and PVA/HA/CH/HAP) promote proliferation of WI38 cells in a concentration-dependent manner, compared to control NFs after 1, 3 and 5 days of cell treatment with different concentrations of 1, 2, 3, 4 and 5 mg/ml, as shown in Fig. 5. Notably, NFs containing HAP *e.g.* PVA/HA/HAP and PVA/HA/CH/HAP composite NFs recorded high cell viability ≥100% at all tested concentrations on WI38 cells. Such promotion of the cell proliferation can be explained by synergistic effect of both HAP and HA, that might reflect acceleration of wound healing activity. This speculation was based on the fact that, HAP was extensively used for versatile biotechnological sectors; such as tissue regeneration, biomedicine medical imaging, hard tissue (bone) repair, and drug delivery application [38,39]; additionally, HA has been displayed a vital physiological role in cell proliferation and growth. Current results are consistent with those obtained by Yang et al. [40], who demonstrated that HAP NPs have an excellent stimulatory effect on osteogenic differentiation of hMSCs as revealed by enhanced expression of bone-related markers. In contrast, Wang et al. [41] revealed that HAP NPs/polyamide composite scaffolds have no negative effects on the cell proliferation, adhesion, and osteogenic differentiation of rabbit bone marrow-derived mesenchymal stem cells. Moreover, Hussein et al. [29] demonstrated that the embedded CNCs nanofibers with PVA/HA loaded-L-arginine which promoted the cell viability proliferation and adhesion of both WI38 and HFB-4 cells.

3.11. Cell adhesion test onto nanofiber scaffolds

Adhesion activity of WI38 cells onto tested nanofibers surfaces are presented in Fig. 6 with varied concentrations of 1, 2 and 4 mg/ml of NFs at different time intervals of 0.5, 2, 4 and 6 h, as compared to control group. Our results showed that all tested NFs provided a brilliant cell adhesion even after extending the contact period of NFs with tested cells. In addition, PVA/HA/HAP NFs displayed the highest cell adhesion behavior at all tested concentrations in time-dependent manner, owing to the huge surface area of NFs, in addition incorporation of HAP probably permitted adhesion of high density adsorbed growth factors, cells or proteins [42]. Recently, Gupta et al. [43] indicated that HA consider a vital substrate to be used in cell adhesion application due to its capability to interact with certain adhesion molecules expressed on cell membrane like membrane glycoprotein (CD44). Furthermore, Shi et al. [44] found that there is an increase in the expression levels of eEF1Bα, γ-actin, and adhesion-associated proteins laterally with stimulation of cell adhesion in case of HAP-coated silicone rubber, compared to non-coated one. Our findings suggest that cell adhesion behavior

might be slightly improved by the synergistic effect of both HA and HAP incorporated in nanofiber scaffolds.

4. Conclusions

In conclusion, obtained results support a successful application of electrospun PVA/HA NFs by electrospinning technique, where chitosan and HAP were also successfully incorporated into NF mats for improving the whole properties of nanofiber scaffolds. Obtained results presented that, NF mats have a high hydrophilic and porous 3D nanofibrous network structure similar to that found in human native extracellular matrix, in particular scaffolds containing HAP. As observed, incorporation of chitosan into NFs enhanced significantly swellability, protein adsorption, haemocompatibility and antimicrobial activity of NFs mats. However, incorporation of HAP into NFs reduced markedly the swellability, enhanced the mechanical/thermal stability, and improved the adhesion and proliferation behavior of WI38 cells onto NFs surfaces. It is assumed that, PVA/HA/HAP NFs demonstrated clinical relevance for application in cases with bone damaged; particularly in craniofacial skeleton [5,45]. NFs composed of PVA/HA/CHCH/HAP scaffold can be used as a bioactive component in a composite scaffold or with a fixation device to provide the necessary biocompatibility support for promising biomaterials.

Author's statement

Samar A. Salim: Methodology, investigation, and writing-original draft, Samah A. Loutfy: Visualization, and resources, Esmail M. El-Fakharany: Methodology, formal analysis and investigation, Tarek H. Taha: Methodology and investigation, Yasmein Hussein: Validation; and Elbadawy A. Kamoun: Methodology, investigation, resources, writing-original draft and writing-review & editing. All authors approve the publication of the manuscript in the current version.

Declaration of competing interest

The authors declare no competing or financial interests.

References

[1] C.D. Weber, F. Hildebrand, P. Kobbe, R. Lefering, R.M. Sellei, H.-C. Pape, D.G. U. TraumaRegister, Epidemiology of open tibia fractures in a populationbased database: update on current risk factors and clinical implications, Eur. J. Trauma Emerg. Surg. (2018) 1–9.

[2] P.V. Giannoudis, H. Dinopoulos, E. Tsiridis, Bone substitutes: an update, Injury 36 (2005) S20–S27.

[3] E. Guerado, E. Caso, Challenges of bone tissue engineering in orthopaedic patients, World J. Orthoped. 8 (2017) 87.

[4] R.R. Betz, Limitations of autograft and allograft: new synthetic solutions, Orthopedics 25 (2002) S561–S570.

[5] F. Salamanna, D. Contartese, N. Nicoli Aldini, G. Barbanti Brodano, C. Grioni, A. Gasbarrini, M. Fini, Bone marrow aspirate clot: a technical complication or a smart approach for musculoskeletal tissue regeneration, J. Cell. Physiol. 233 (2018) 2723–2732.

[6] A. Jouybar, E. Seyedjafari, A. Ardeshirylajimi, A. Zandi-Karimi, N. Feizi, M. M. Khani, I. Pousti, Enhanced skin regeneration by herbal extract-coated poly-L-lactic acid nanofibrous scaffold, Artif. Organs 41 (2017) E296–E307.

[7] J.-l. Sun, K. Jiao, L.-n. Niu, Y. Jiao, Q. Song, L.-j. Shen, F.R. Tay, J.-h. Chen, Intrafibrillar silicified collagen scaffold modulates monocyte to promote cell homing, angiogenesis and bone regeneration, Biomaterials 113 (2017) 203–216.

[8] J. Melke, S. Midha, S. Ghosh, K. Ito, S. Hofmann, Silk fibroin as biomaterial for bone tissue engineering, Acta Biomater. 31 (2016) 1–16.

[9] F. Pournaqi, A. Ghiaee, S. Vakilian, A. Ardeshirylajimi, Improved proliferation and osteogenic differentiation of mesenchymal stem cells on polyaniline composited by polyethersulfone nanofibers, Biologicals 45 (2017) 78–84.

[10] M.F. Abazari, F. Soleimanifar, M.N. Aleagha, S. Torabinejad, N. Nasiri, G. Khamisipour, J.A. Mahabadi, H. Mahboudi, S.E. Enderami, E. Saburi, PCL/PVA nanofibrous scaffold improve insulin-producing cells generation from human induced pluripotent stem cells, Gene 671 (2018) 50–57.

[11] M. Ravi, V. Paramesh, S.R. Kaviya, E. Anuradha, F.D.P. Solomon, 3Dcell culture systems: advantages and applications, J. Cell. Physiol. 230 (2015) 16–26.

[12] C. Murphy, K. Kolan, W. Li, J.A. Semon, D.E. Day, M.-C. Leu, 3D Bioprinting of Stem Cells and Polymer/Bioactive Glass Composite Scaffolds for Bone Tissue Engineering, 2017.

[13] H. Yi, F.U. Rehman, C. Zhao, B. Liu, N. He, Recent advances in nano scaffolds for bone repair, Bone Res 4 (2016) 16050.

[14] S.R. Motamedian, S. Hosseinpour, M.G. Ahsaie, A. Khojasteh, Smart scaffolds in bone tissue engineering: a systematic review of literature, World J. Stem Cell. 7 (2015) 657.

[15] M.I. Baker, S.P. Walsh, Z. Schwartz, B.D. Boyan, A review of polyvinyl alcohol and its uses in cartilage and orthopedic applications, J. Biomed. Mater. Res. B Appl. Biomater. 100 (2012) 1451–1457.

[16] A. Mustafa, A.M. Ionescu, M. Cherim, R. Sîrbu, Chitosan applications used in medical therapy of tissue regeneration, European Journal of Interdisciplinary Studies (2) (2016) 271–278.

[17] M. Rodríguez-Vázquez, B. Vega-Ruiz, R. Ramos-Zúñiga, D.A. Saldaña-Koppel, L. F. Quiñones-Olvera, Chitosan and its potential use as a scaffold for tissue engineering in regenerative medicine, BioMed Res. Int. (2015), 2015.

[18] S. Kim, Competitive biological activities of chitosan and its derivatives: antimicrobial, antioxidant, anticancer, and anti-inflammatory activities, International Journal of Polymer Science (2018), 2018.

[19] C. Longinotti, The use of hyaluronic acid based dressings to treat burns: a review. Burn, Trauma 2 (2014) 162–168.

[20] H. Debels, M. Hamdi, K. Abberton, W. Morrison, Dermal matrices and bioengineered skin substitutes: a Critical review of current options, Plast. Reconstr. Surg. Glob. Open 3 (2015) e284.

[21] V. Voinchet, P. Vasseur, J. Kern, Efficacy and safety of hyaluronic acid in the management of acute wounds, Am. J. Clin. Dermatol. 7 (2007) 353–357.

[22] S.P. Zhong, D. Campoccia, P.J. Doherty, R.L. Williams, L. Benedetti, D.F. Williams, Biodegradation of hyaluronic acid derivatives by hyaluronidase, Biomaterials 15 (1994) 359–365.

[23] C. Xu, R. Inai, M. Kotaki, S. Ramakrishna, Electrospun nanofiber fabrication as synthetic extracellular matrix and its potential for vascular tissue engineering, Tissue Eng. 10 (2004) 1160–1168.

[24] H. Yoshikawa, A. Myoui, Bone tissue engineering with porous hydroxyapatite ceramics, J. Artif. Organs 8 (2005) 131–136.

[25] L. Russo, F. Taraballi, C. Lupo, A. Poveda, J. Jiménez-Barbero, M. Sandri, A. Tampieri, F. Nicotra, L. Cipolla, Carbonate hydroxyapatite functionalization: a comparative study towards (bio)molecules fixation, Interface Focus 4 (1) (2014), 20130040.

[26] Y. Chen, J. Yu, Q. Ke, Y. Gao, C. Zhang, Y. Guo, Bioinspired fabrication of carbonated hydroxyapatite/chitosan nanohybrid scaffolds loaded with TWS119 for bone regeneration, Chem. Eng. J. 341 (2018) 112–125.

[27] A.C. Queiroz, J.D. Santos, F.J. Monteiro, I.R. Gibson, J.C. Knowles, Biomaterials 22 (2001) 1393.

[28] W.C. Lin, D.G. Yu, M.C. Yang, Colloids Surf., B 47 (2006) 43.

[29] Y. Hussein, E.M. El-Fakharany, E.A. Kamoun, S.A. Loutfy, R. Amin, T.H. Taha, S. A. Salim, M. Amer, Electrospun PVA/hyaluronic acid/L-arginine nanofibers for wound healing applications: nanofibers optimization and in vitro bioevaluation, Int. J. Biol. Macromol. 164 (2020) 667–676.

[30] A.J. Rahyussalim, T. Kurniawati, D. Aprilya, R. Anggraini, G. Ramahdita, Y. Whulanza, Toxicity and biocompatibility profile of 3D bone scaffold developed by universitas Indonesia: a preliminary study, in: AIP Conference Proceedings, vol. 1817, 2017, pp. 1–6, 02004.

[31] Parinita Agrawal, Krishna Pramanik, Chitosan-Poly(vinyl Alcohol) Nanofibers by Free Surface Electrospinning for Tissue Engineering Applications, 2016, pp. 1738–2696.

[32] F. Croisier, C. Jérôme, Chitosan-based biomaterials for tissue engineering, Eur. Polym. J. 49 (2013) 780–792.

[33] P.C. Sergio, B.B. Andrés, B.L. Cristian, S.P. Hugo, N.M. Diana, V.B. Andrea, M. F. Diana, M. Lukas, Synthesis and characterization of poly(vinyl alcohol)-chitosan-hydroxyapatite scaffolds: a promising alternative for bone tissue regeneration, Molecules 23 (2018) 2414.

[34] R. Ghiska, M.P. Debie, F.A. Muh, A. Rowi, S. Nofrijon, H.Y. Akhmad, The effect of hydroxyapatite addition on the mechanical properties of polyvinyl alcohol/chitosan biomaterials for bone scaffolds application, AIP Conference Proceedings 1933 (2018), 020006.

[35] M. Burkatovskaya, G.P. Tegos, E. Swietlik, T.N. Demidova, A. Castano, M. R. Hamblin, Use of chitosan bandage to prevent fatal infections developing from highly contaminated wounds in mice, Biomaterials 27 (2006) 4157–4164.

[36] T. Jiang, E. Carbone, K. Lo, C. Laurencin, Prog. Polym. Sci. 46 (2015) 1–24.

[37] M.R. Hwang, J.O. Kim, J.H. Lee, Y. Kim, J.H. Kim, S.W. Chang, S.G. Jin, J.A. Kim, W.S. Lyoo, S.S. Han, S.K. Ku, C.S. Young, H.G. Choi, Gentamicin-loaded wound dressing with polyvinyl alcohol/dextran hydrogel: gel characterization and in vivo healing evaluation, AAPS Pharm. Sci. Technol. 11 (3) (2010) 1092–1103.

[38] M. Epple, K. Ganesan, R. Heumann, J. Klesing, A. Kovtun, S. Neumann, V.J.J. C. Sokolova, Application of calcium phosphate nanoparticles in biomedicine, J. Mater. Chem. 20 (1) (2010) 18–23.

[39] C. Zhou, Y. Hong, X. Zhang, Applications of nanostructured calcium phosphate in tissue engineering, Biomaterials science 1 (10) (2013) 1012–1028.

[40] X. Yang, Y. Li, X. Liu, R. Zhang, Q. Feng, In vitro uptake of hydroxyapatite nanoparticles and their effect on osteogenic differentiation of human mesenchymal stem cells, Stem Cell. Int. (2018), 2018.

[41] H. Wang, Y. Li, Y. Zuo, J. Li, S. Ma, L. Cheng, Biocompatibility and osteogenesis of biomimetic nano-hydroxyapatite/polyamide composite scaffolds for bone tissue engineering, Biomaterials 28 (22) (2007) 3338–3348.

[42] B.P. Antunes, A.F. Moreira, V.M. Gaspar, I.J. Correia, Chitosan/arginine–chitosan polymer blends for assembly of nanofibrous membranes for wound regeneration, Carbohydr. Polym. 130 (2015) 104–112.

[43] R.C. Gupta, R. Lall, A. Srivastava, A. Sinha, Hyaluronic acid: molecular mechanisms and therapeutic trajectory, Frontiers in Veterinary Science 6 (2019) 192.

[44] X.H. Shi, S.L. Wang, Y.M. Zhang, Y.C. Wang, Z. Yang, X. Zhou, Z.Y. Lei, D.L. Fan, Hydroxyapatite-coated sillicone rubber enhanced cell adhesion and it may be through the interaction of EF1β and γ-Actin, PloS One 9 (11) (2014) e111503.

[45] Garcia Garcia Alejandro, Multiscale Analysis of Multi-Layered Tissues Constructs: Interfaces in the Musculo-Skeletal System Based on Tissue Engineered *Osteotendinous* Junctions, Ph.D. thesis, Université de Technologie de Compiègne, Switzerland, 2020.